IN-SITU REPAIR OF COMPOSITE SANDWICH STRUCTURES USING CYANOACRYLATES

Jack F. Cullinan[a], Paul Velut[c], Veronique Michaud[b], Michael R. Wisnom[a] and Ian P. Bond[a]

[a]*Advanced Composite Centre for Innovation & Science (ACCIS), Department of Aerospace Engineering, University of Bristol, Bristol, BS8 1TR, United Kingdom*
[b]*Laboratory of Polymer and Composite Technology (LTC), Ecole Polytechnique Federale de Lausanne (EPFL), CH-1015, Switzerland*
[c]*Décision S.A., Lausanne, CH-1024, Switzerland*

Corresponding Email: jack.cullinan@bristol.ac.uk

Abstract

A novel method for the in-situ repair of composite sandwich structures using microvascular networks and cyanoacrylate (CA) adhesive systems has been presented. Upon a damage event, the vascules become ruptured, providing a route for the introduction of adhesive directly into the damage site. The efficacy of the two repair agents was first assessed under static and fatigue conditions using a modified double cantilever beam (DCB) method. Once baseline fracture behaviour of the cyanoacrylates has been established, they were further assessed by injection into a series of pre-damaged T-joint specimens. The presence of the vasculature was shown to have no detrimental impact on mechanical performance, whilst both of the cyanoacrylates were shown to be highly effective in the recovery of stiffness and ultimate strength of the T-joint specimens.

Keywords: A. Sandwich Structures, B. Fatigue, B. Damage Tolerance, Self-Healing

1. Introduction

The increased use of composites has been accompanied by a corresponding trend towards the use of larger integrated composite structures. By mitigating the need for bonding or mechanical fastening of smaller components, designers are able to better realise the specific capabilities of fibre reinforced materials. There are, however, many occasions when the cost or complexity of manufacturing fully integrated structures may be prohibitive, thereby necessitating the use of secondary bonding. One such occasion is in the secondary bonding of internal features in marine structures.

In naval architecture, particularly performance sporting crafts, external structures such as the hull are often manufactured as single components or as a small number of larger bonded components. Internal supports such as ribs, stiffeners and bulkheads (collectively known as scantlings) are then secondary bonded using a fibre reinforced polymer (FRP) fabric overlaminate or simply using unreinforced resin fillets at the T-joint intersections. Due to the nature of the mechanical loading of these vessels, the internal scantlings can be prone to both fatigue and impact damage during service. Once damage has occurred, access to the damage site is often impaired by internal substructure, and repairs often require lengthy periods in dock. As a result, even relatively simple repairs can become costly and non-trivial. A requirement, therefore, has been identified to develop a method to reliably repair these structures in-situ, thereby mitigating the need for invasive repairs or for the vessel to be taken out of service.

The T-joint configuration was chosen for this study as it is a good lab scale analogue for many common types of marine joint. A typical sandwich T-joint consists of four components: two sandwich panels, the *web* and *substrate,* which are co-bonded together using a FRP *overlaminate* and/or a *deltoid* fillet (see Fig.1).

The influence of joint geometry on failure of composite T-joints is well established in the literature. Under 90° tensile (pull-off) loading, cracking within the deltoid and/or delamination of the adjacent overlaminate region [1] is a commonly observed failure mechanism. Increasing the thickness of the overlaminate tends to promote delamination within the root of the overlaminate, whilst decreasing the thickness tends to promote deltoid failure [2,3]. Whilst the majority of failures occur within the deltoid region, short overlaminate lengths have also been shown to promote core failure of the substrate and web [4].

The effect of different load cases has also been examined, such as fatigue, compression and off-axis bending. Crack initiation location under fatigue was similar to that observed under quasi-static loading; however, damage initiation loads were lower and crack advancement was more progressive in nature [5,6]. Failures under compression (-0°, Fig. 1.) are also largely similar to failures under static tension. Damage initiation is often observed in the deltoid region, although, depending on clamping conditions buckling modes can be introduced causing core failure [1] and delamination of the web [7]. Under off-axis bending (rotation of the web section towards the substrate), failure is primarily observed within the radiused section of the overlaminate and adjacent deltoid region [8,9].

In addition to understanding the factors governing failure in conventional T-joints, attempts have also been made to optimise joint strength using a range of methods. Such methods include novel geometries [10–13], novel layups [14,15] and through thickness reinforcement techniques [16,17]. A detailed review of T-joint failure mechanisms is beyond the scope of this paper, however, a number of key observations have been discussed previously for completeness.

In contrast to the wealth of literature available regarding the design and failure of T-joints, relatively little has been published in the area of T-joint and structural repair. The lack of standardised repair approaches across boat manufacturers and classification societies can result in considerable variation in repair procedures implemented. Repair techniques for flat surfaces tend to be highly invasive, requiring extensive material removal and the application of either a scarfed (patch) or externally bonded (doubler) repair. Repair of more complex structures such as stiffeners or ribs is considerably more challenging, although recent developments with metallic repairs in the aerospace sector have made progress towards simplification of these procedures [18].

1.1. Vascular In-Situ Repair / Self-healing

Inspired by the ability of biological systems to autonomously repair damage, self-healing technologies aim to repair damage in-situ, allowing for rapid response to a damage event. In the case of self-healing FRPs, self-healing is generally achieved using one of three main strategies: *microcapsule-based* [19,20], *vascular* [21–23] or *intrinsic* [24,25] self-healing.

The microcapsule-based approach utilises a discrete encapsulated repair agent contained in a rigid shell and embedded within the matrix. Upon a damage event, cracks will interact with the capsules, causing them to rupture, allowing the repair agent inside to leak out onto the damage plane and restore functionality. Vascular systems are similar, but where the two strategies differ is that vascular systems are continuous, capable of delivering much greater volumes of repair agent typically from a remote reservoir.

Intrinsic systems are distinct in that they do not rely on liquid phase repair agents. Instead, repair is achieved through the intrinsic ability of the material to self-adhere, either through strong secondary bonding or mechanical interlocking of the embedded self-healing materials. It is worth noting that all of these systems aim to restore functionality to either the matrix or interphase regions and not to the fibre reinforcement phase.

Examining vascular systems in more detail, it has been shown that the deployment of microchannels into a fibre reinforced system must be carefully considered. Norris *et al.* have shown that parameters such as the vascule diameter [26,27] and orientation relative to the fibre reinforcement [28] strongly affect the ultimate performance of the composite. A key finding is that alignment of the vasculature in the fibre direction is highly preferable as it eliminates the requirement to cut plies and introduce fibre discontinuities into the system. In the case of T-joints, the deltoid region (see Fig. 1) is an ideal candidate location for the deployment of vascules. It is known to be prone to damage, it is challenging to repair and the absence of transverse fibres in this region lends itself well to vascule integration.

Note: The terms self-healing and in-situ repair are often used interchangeably but are not necessarily synonymous. The primary difference between the two terms is that self-healing implies a degree of autonomy beyond that of the system presented herein. As the vascules are simply used as networks by which to effect a repair in-situ, the term ‘in-situ repair’ is the preferred terminology used in this paper.

2. Experimental

The aim of this paper is to experimentally demonstrate the efficacy of cyanoacrylates (CA) as a repair agent in composite structures. Tests were first performed on vascularised and unvascularised T-joints to determine their failure mechanisms. Specimens were then infused with a CA, cured and retested. Both static and fatigue recovery was achieved; however, a better understanding of the recovery mechanisms was required. A modified Mode I double cantilever beam (DCB) method with dissimilar beam materials was therefore used. This specimen was intended to mimic the interface between the substrate/web and overlaminate (the primary failure location observed in T-joint tests). This method was used to numerically quantify the efficacy of the CAs and is a robust tool for the identification of candidate repair agents. As the two adherends were heterogeneous it was necessary to first determine the apparent stiffness of the constituent materials using a 4 point bend test. Once the correlation between ply count and apparent stiffness for the two materials had been established, DCBs were manufactured and tested in both static and fatigue. The DCB and T-joint results were then compared to verify the correlation between apparent toughness and repair efficacy.

2.1. Materials

All T-joint specimens were manufactured from marine-grade carbon fibre/epoxy materials. The substrate and web plates were pre-manufactured as per the manufacturers recommended curing cycle. The web and substrate were then secondary bonded together using vacuum assisted wet layup. The sandwich panels were made of a combination of woven and unidirectional (UD) T700/VTM 264 prepreg (Cytec, UK) co-bonded to 15mm Divinycell HP200 PVC/Polyurea foam core (Diab Group, Sweden) with a protective layer of peel ply on both top and bottom surfaces. All panels were cured according to the manufacturer’s recommendations. Foam core material was kept in a desiccated environment prior to sandwich panel fabrication. The web and substrate were first joined by a 5mm radius Spabond 340lv thixotropic epoxy fillet (Gurit,

Switzerland) and allowed to cure for 24 hours at ambient temperature. This was formed by direct injection of epoxy through a pneumatic mixing nozzle, with excess material removed via a 5mm radius scraping tool. In the case of vascularised specimens, a 1mm diameter nylon monofilament was placed in the deltoid at the corner of the web/substrate junction prior to injection of the epoxy fillet and removed after curing (see Fig.2). The peel ply protective film was removed immediately prior to application of a Resoltech 3350T/3357T (Resoltech, France) structural adhesive. Immediate application of the structural adhesive mitigates the need for additional surface preparation and is in line with industrial practice. Biaxial carbon fibre fabric (400gsm, Formax, UK) was preimpregnated with Elan-tech EC152/W152 marine grade epoxy (Elantas, Italy) and manually applied to the T-joint surface. The specimens were then vacuum consolidated and allowed to cure for 24 hours at ambient temperature before post curing at 50°C for 16 hours. The specimen layup is given in Table 1.
After post curing the T-joint specimens were cut to nominal dimensions of 25 x 180 x 120mm (w x l x h) using a diamond saw. Specimens were abraded with 400 grit Silicon carbide abrasive paper to remove machining striations and stored in a desiccated environment prior to testing.

Flexure specimens were manufactured using the same materials as for the T-joint specimens. Prepreg specimens were manufactured from woven material, whilst wet layup specimens were manufactured from a combination of woven and unidirectional material as shown in Table 2. Wet layup specimens F5 and F6 used alternating 400/300gsm UD material (Gurit, UK. see note 1). Flexure specimen length was dictated by a span to thickness ratio of 60:1 +20% allowable overhang (see Table 3). DCB specimens were laid up using the same manufacturing method described previously for the T-joints; namely, premanufactured prepreg substrate subject to secondary bonding.

Instead of a sandwich panel substrate, the prepreg component of the DCB specimen was manufactured exclusively from woven T700/VTM 264, as used in the skin of the sandwich panels. A 25µm Polytetrafluoroethylene (PTFE) film insert was used as a crack initiator. The layup is also given in Table 2.

In-situ repair was achieved by manual syringing of cyanoacrylate into the damage plane. In the case of DCB specimens, this was achieved by holding the crack plane open and directly injecting onto the fracture surface. In the case of T-joints, all repair agents were injected via the in-situ vasculature whilst not under load (i.e. crack closed position).

After pre-cracking, a Loctite 7457 (Henkel, Ireland) amine based activator was first syringed into the fracture plane of both the DCB and T-joint specimens before being left for 20 minutes to dry fully at ambient temperature. The purpose of the activator was to provide additional hydroxyl groups to the fracture plane in order to maximise polymerisation. Next, approximately 2ml of cyanoacrylate was manually syringed onto the crack plane to excess (i.e. complete coverage) and immediately clamped closed using spring clamps. Bondline thickness was dictated by the clamping pressure and was nominally identical between repaired samples. In the absence of a standardised repair agent, two rubber toughened cyanoacrylates were investigated during this study, Loctite 435 (LT435) and Loctite 480 (LT480) (Henkel, Ireland). These systems were selected for their compatibility with polymeric substrates, low viscosity (200mPa.s) and relatively slow curing times (10-50 seconds). Specimens were allowed to cure at ambient temperature for a minimum of 72 hours prior to testing. All infused specimens, static and fatigue, were pre-cracked under quasi-static conditions before subsequent retesting.

2.2. Mechanical Test Methods

Four-point bend tests (1/2 configuration) were carried out in accordance to ASTM D6272-10 [29] on a Shimadzu Autograph AGS-X with a ±1kN static load cell. Both the loading and support rollers were 10mm in diameter stainless steel, and the span width is given in Table 3. Beam displacement was measured using a video gauge. The crosshead displacement rate was calculated to maintain a constant strain rate in the outer fibres of 0.01mm/mm. Specimens were tested until failure or until an arbitrary crosshead displacement, no less than 15mm. The tangent modulus of elasticity was obtained using Equation 1 as follows:

$$E_B = \frac{0.17 L_s^3 m}{b d^3} \tag{1}$$

(Where: E_B = modulus of elasticity in bending, MPa, L_s = support span, mm, b = width of the beam, mm, d = depth of beam, mm, m = slope of the tangent to the initial straight-line (steepest initial straight line portion of the load/displacement curve))

A schematic of the asymmetric DCB specimen is given in Fig. 3. In order for this method to approach pure Mode I, the bending stiffness of the two beams must be closely matched. Taking a cantilever beam of rectangular cross section subject to end loading, the following relationship must be satisfied:

$$\left(\frac{Pl^3}{3E} \cdot \frac{12}{bt^3}\right)_{overlaminate} = \left(\frac{Pl^3}{3E} \cdot \frac{12}{bt^3}\right)_{substrate} \tag{2}$$

Re-arranging Equation 2 and cancelling common terms yields Equation 3:

$$E_o t_o^3 = E_s t_s^3 \tag{3}$$

Static and fatigue DCB & T-joint tests were performed on an Instron 8872 servo-hydraulic test machine with a ±1kN and ±5kN dynamic load cells respectively. Static tests for both specimens were performed at a crosshead velocity of 5mm/min until 40mm crack propagation (DCB) or initial failure (T-joint) was achieved. Both the peak load at crack initiation (F_{max}) and the corresponding displacement (δ_{max}) were recorded. After static pre-cracking, specimens were injected with a repair agent and allowed to cure as described previously. Static tests on repaired DCB specimens were also performed until 40mm crack propagation had been achieved. This ensured that the measured toughness was representative of interfacial recovery of the repair area and not the host substrate. For consistency, all fatigue samples were first pre-cracked under static conditions prior to repair and subsequent re-testing. Fatigue DCB tests were performed at 7Hz and 70% intensity ($\delta/\delta_{max} = 0.7$). The loading intensity of the T-joints specimens was reduced to account for viscoelastic effects of the foam core. As a result, T-joint tests were performed at 4Hz and 50% intensity. All fatigue tests were performed under displacement control at an R-ratio of R=0.1. Fatigue tests on repaired samples (both DCB and T-joint) were performed under the same crack opening displacements as the virgin samples for direct comparison purposes.

T-joint tests were performed in tension by applying a pull-off load to the vertical web section of the overlaminate (see Fig.4). Specimens were carefully clamped so as to minimise the potential for core crushing within the clamping region. The perpendicular substrate section was constrained by two 10mm diameter loading rollers placed 130mm apart. The loading span was chosen so as to promote bending failure of the joint, as observed in literature, and minimise the potential for core failure of the substrate.

The exact load case experienced by the T-joint prior to failure is somewhat irrelevant to this work. It is assumed, therefore, that the manner in which damage occurred in the joint does not affect the ability of the vascular system to implement a repair. This paper will instead focus on the engineering challenges associated with the introduction of vascular self-healing infrastructure into marine structures, and the subsequent repair of said structures. As a result, only the relatively simple load case of a T-joint subject to 90° tensile loading has been considered herein.

3. Results & Discussion

3.1. Flexure Tests

The flexural stiffness of the various flexure specimens was calculated as per Equation 3, and is given in Fig. 5. From these results it was possible to identify the substrate/overlaminate combination that was most closely matched, in order to achieve a balanced DCB specimen. From Fig. 5 it can be seen that of the specimens tested, F3 (substrate) and F4 (overlaminate) were most closely matched. However, there is still a miscorrelation in apparent stiffness of approximately 33% between the two layups. Additionally, combining the two beam thicknesses would result in an anticipated DCB specimen thickness of 2.65mm. As this is below the minimum thickness recommended by the relevant standard (ASTM D5528 [30]), a thicker configuration was required.

As stiffness is highly sensitive to thickness, it was apparent that an increase in specimen thickness was necessary so as to minimise the influence of stiffness differentials. It was, therefore, necessary to estimate the number of plies required to match the stiffness of the substrate to that of one of the thicker overlaminate beams (F5 or F6).

Using a simple linear projection, it was possible to estimate the influence of increased ply count on both thickness and apparent modulus. Substituting this information into Equation 3, it was anticipated that increasing the number of plies in the substrate from 5 (F3) to 8 plies (FP3) would result in an apparent stiffness correlation similar to that of

F5 (see Fig.5). Here it would be expected that there would be a nominal stiffness disparity of approximately 8.5% between the two beams. Although not identical, a difference of less than 10% would be expected to have only a small influence on the stress state at the crack tip and was, therefore, deemed acceptable. The negligible stiffness differential was later confirmed by measurement of the beam deflections during DCB testing. DCB specimens consisting of FP3 and F5 beams were used during the fracture tests as outlined in Table 2.

3.2. Mode I (DCB) Fracture Tests

It was first necessary to verify that the flexural stiffness of the two halves of the DCB specimen were balanced. This was achieved by analysing the variance in external angle between the load line, crack tip, and specimen end as shown in Fig. 6. A difference in beam deflection angle of approximately 1.5% ±0.2% between the two substrates verifies that the beam stiffnesses were closely matched. As a result, it can be reasonably concluded that the fracture plane is experiencing near pure-Mode I failure.

Baseline DCB tests demonstrated highly stick-slip crack propagation behaviour as shown in Fig. 7(a). After an initial load drop the delamination became pinned at a certain crack length, until reaching a critical strain energy release rate, and the crack propagated once more. It can also be seen that both the peak initiation and maximum propagation loads varied across samples. Although a characteristic behaviour of the system presented, this failure mechanism provides challenges in numerically quantifying fracture toughness. As a result, only initiation strain energy release rate (G_{IC}) values of the control specimens have been quoted herein. Initiation G_{IC} was determined from the maximum load at initial failure, and these were of the order of 240-600J/m^2 (see Table 4).

The failure behaviour of the repaired specimens was somewhat different to that of the control. Both CA systems were effective in recovering peak initiation loads under static loading, whilst propagation loads and embodied fracture energies were comparable or higher than those of the virgin specimens (see Fig. 7(b) and (c)). Crack propagation was observed to be more progressive in both CA systems than the control, allowing for an estimation of the propagation fracture toughness. The propagation energy release rates of Loctite 480 (circa 1250-1500 J/m^2) were considerably higher than that of Loctite 435 (circa 750J/m^2). The difference between the two CA systems and the control may be better explained by examining the fracture morphology.

Fractographic analysis of the control specimens revealed that primary failure occurred along the fibre/matrix interface of the overlaminate beams. Occasionally damage could be seen to propagate locally to the opposing face, most typically in locations associated with crack pinning or 'sticking' of the crack front. Interfacial failure was observed leaving a mirror image imprint on the opposing face as shown in Fig.8(b) and Fig.8(a) respectively.

Crack propagation within the repaired systems changed from highly interfacial to primarily cohesive failure of the CA interlayer. Loctite 435 systems exhibited elongated riverlines aligned in the direction of crack propagation, indicative of a pseudo-ductile material response, as shown in Figs.8(c) and (d). In contrast, the Loctite 480 system showed less ductile features and a significantly more textured morphology. Uniform inclusions of 100-200μm diameter were also noted in the 480 system, as shown in

Fig.8(e). Due to the uniformity and dispersion it is speculated that these inclusions were either the remnants of the rubber toughening phase or voids left from volatile outgassing during curing. Both CA systems appeared to be highly effective in wetting out the fracture plane, with only minor voidage noted in either specimens.

Fatigue Tests

Baseline crack growth Paris plots (d*a*/d*N*) for the control and repaired DCB specimens are given in Figs. 8(a) and (b). These were determined by measuring the peak load per cycle and using a compliance calibration method to back calculate the crack length. Propagation rates and ultimate crack lengths were observed to vary somewhat between samples, as seen in Fig 8(a). In all cases, crack propagation rates were high during the initial phase of testing before decaying until runout, whilst ultimate crack lengths varied from 13-20mm. This variable crack propagation behaviour of the control material is consistent with the static results observed in Fig. 7(a).

In contrast to the control specimens, failure of the CA infused specimens was far more consistent between samples. Initiation G_{IC} values were of the order of 154±22J/m^2 and 358±28J/m^2 (LT435 & LT480 respectively), and steady state growth decay also exhibited less variability. Comparing exponents in Fig.9(a) and (b), it can be seen that damage progression was most rapid in the LT435 system. The LT480 system, by contrast, performed comparably to the best results observed in the controls. All samples achieved an ultimate crack length of approximately 26mm at run out. Based on these results, the well behaved nature of the LT480 system make it an ideal candidate material for the in-situ repair of composite structures.

3.3. T-Joint Tests

Two rounds of T-joint tests were performed. The first round of testing examined the static response of the T-joints to vasculature and CA repair. The second round of testing focused exclusively on the fatigue response of the joints and the efficacy of CA as a repair agent. An overview of the static test results is given in Table 5. From these results it was observed that the presence of the vasculature within the structure had no statistically significant influence on the static strength of the joint. In a small number of cases, skin failure of the bottom surface of the substrate occurred, resulting in core crushing and localised delamination. In the majority of cases, however, failure was observed to initiate at the radiused deltoid section of the overlaminate before propagating along the overlaminate/substrate interfaces along both sides of the specimen (see Fig.4). This failure mechanism resulted in reliable rupturing of the vascular micro-channels, essential for effective repair.

Damage patterns after infusion were very similar to that of the virgin material. Cracks were seen to initiate within the deltoid region and propagate rapidly along the substrate/overlaminate interface. Examining the load bearing recovery it can be see than healing efficiencies ($\eta = \frac{P_{max,repaired}}{P_{max,virgin}} x\ 100$) of 70% and 80% were achieved using LT435 and LT480 respectively, whilst a relatively modest recovery of ultimate strain was achieved as shown in Fig.10. Significantly, almost complete recovery of joint stiffness was achieved. This is an important result given many structures are subject to stiffness- and not strength-driven design constraints. Examination of the fracture surfaces revealed that both systems were highly effective in wetting out the entirety of the damage plane (typically 15-25mm from the vascule location).

Fatigue Tests

Under fatigue, as observed in Fig. 11, in all cases the stiffness of the T-joint specimens decays as a function of the number of cycles, until a critical point, after which rapid failure ensues. In the case of the control specimens (see Fig. 11) an initial reduction in loadbearing capacity, typically during the first 1000 cycles, of the order of 2-4% was observed. Damage was observed to be progressive after this point, with visible damage (minor cracking in the radiused section of the overlaminate) occurring from approximately 10,000 cycles. As the specimens approached the ultimate fatigue life, damage progression was seen to accelerate until a single catastrophic failure event caused rapid delamination along the overlaminate/substrate interface.

Failure mechanisms of the CA infused T-joint samples were very similar to those of the control samples. Minor interlaminar cracking and disbonding of the overlaminate/substrate interface was observed in both CA systems prior to ultimate failure. Fatigue recovery of the LT435 system was modest, whilst the LT480 system successfully retained over 80% of pristine strength at 10,000 cycles. Comparing ultimate fatigue lives (defined as the number of cycles to catastrophic failure), it can be observed that both CA systems gave lower lives than that of the control samples. The mean number of cycles to failure of the control specimens was approximately 58,900 cycles. In contrast, fatigue lives of approximately 5,000 and 18,500 cycles were observed with LT435 and LT480 respectively. Although complete recovery was not achieved, such an improvement may allow for the safe extension in operation of a vascularised structure well beyond its original design life.

4. Conclusion

A novel method for the in-situ repair of composite T-joints using microvascular networks and cyanoacrylate (CA) adhesive systems has been presented. Vascules were introduced into the deltoid region and were shown to have no statistically significant influence on mechanical performance of the T-joints. In the majority of cases vasculature was reliably ruptured during mechanical loading, providing a direct route for the introduction of a repair agent to the damage site. The failure mechanisms and effectiveness of the repair agents were assessed using both T-joint structures and Mode I double cantilever beam (DCB) coupons. A modified DCB method using asymmetric beams and dissimilar beam materials was shown to be highly effective in characterising the apparent repair efficacy under both static and fatigue conditions.

Two cyanoacrylate systems were investigated, Loctite 435 and Loctite 480. Both systems were shown to be effective in recovering mechanical performance, resulting in complete recovery of initial apparent strain energy release rate within the experimental variability. Fatigue results demonstrated that of the two systems investigated, Loctite 480 demonstrated the highest initiation fracture toughness and a crack growth rate comparable to that of the virgin sample. When introduced to full T-joint structures, the Loctite 480 system again demonstrated the best static performance, achieving complete recovery of joint stiffness and up to 80% of ultimate joint strength. Under fatigue loading the Loctite 480 system was shown to be highly effective in recovering joint performance, maintaining approximately 82% of undamaged stiffness after 10,000 cycles.

Although application specific optimisation may be required, the low viscosity and ambient temperature cure of CAs make them an ideal material for the rapid-response or pre-emptive repair of composite structures. When combined with in-situ microvascular networks, this strategy shows significant promise as a means for both improving damage tolerance and mitigating the need for traditional, highly invasive repair methods. The deployment of any such system in an industrial setting will be heavily dependent on a number of factors, including: certification requirements, ease of fabrication, environmental compatibility and cost. The methodology presented is robust and simple to implement. Further improvements could be realised by pre-fabrication of the vascular networks for ease of manufacturing.

Acknowledgements

The authors would like to acknowledge the assistance of Ms Federica Sordo (EPFL), Dr Neal Murphy (UCD, Ireland) and Décision S.A. in conducting this research. This project was sponsored by the People Program (Marie Curie ITN) of the European Union's seventh framework program, FP7, grant number 290308 (SHeMat).

References

[1] Shenoi RA, Violette FLM. A Study of Structural Composite Tee Joints in Small Boats. J Compos Mater 1990;24:644–66. doi:10.1177/002199839002400604.

[2] Shenoi R, Hawkins G. Influence of material and geometry variations on the behaviour of bonded tee connections in FRP ships. Composites 1992;23:335–45. doi:10.1016/0010-4361(92)90333-P.

[3] Zimmermann K, Zenkert D, Siemetzki M. Testing and analysis of ultra thick composites. Compos Part B Eng 2010;41:326–36. doi:10.1016/j.compositesb.2009.12.004.

[4] Theotokoglou EE, Moan T. Experimental and Numerical Study of Composite T-Joints. J Compos Mater 1996;30:190–209. doi:10.1177/002199839603000203.

[5] Shenoi RA. Fatigue failure mechanisms in fibre-reinforced plastic laminated tee joints. Int J Fatigue 1995;17:415–26. doi:10.1016/0142-1123(95)98238-X.

[6] Pilipchuk VN, Ibrahim R a. Analysis of crack formation in T-joint structures under dynamic loading. J Vib Control 2010;17:373–90. doi:10.1177/1077546309349851.

[7] Ozes C, Aydin O. Analysis of sandwich t-joints under compression loads in marine applications. Adv Compos Lett 2009;18:67–75.

[8] Phillips H, Shenoi R. Damage tolerance of laminated tee joints in FRP structures. Compos Part A Appl Sci Manuf 1998;29:465–78. doi:10.1016/S1359-835X(97)00081-X.

[9] Hélénon F, Wisnom MR, Hallett SR, Trask RS. Investigation into failure of laminated composite T-piece specimens under bending loading. Compos Part A Appl Sci Manuf 2013;54:182–9. doi:10.1016/j.compositesa.2013.07.015.

[10] Toftegaard H, Lystrup A. Design and test of lightweight sandwich T-joint for naval ships. Compos Part A Appl Sci Manuf 2005;36:1055–65. doi:10.1016/j.compositesa.2004.10.031.

[11] Diler E a., Ozes C, Neser G. Effect of T-Joint Geometry on the Performance of a GRP/PVC Sandwich System Subjected to Tension. J Reinf Plast Compos 2008;28:49–58. doi:10.1177/0731684407081378.

[12] Guo S, Morishima R. Numerical analysis and experiment of composite sandwich T-joints subjected to pulling load. Compos Struct 2011;94:229–38. doi:10.1016/j.compstruct.2011.06.022.

[13] Guo S, Morishima R. Design, analysis and testing of sandwich T-joint structures. 50th AIAA/ASME/ASCE/AHS/ASC Struct Struct … 2009:1–11.

[14] Burns LA, Mouritz AP, Pook D, Feih S. Bio-inspired design of aerospace composite joints for improved damage tolerance. Compos Struct 2012;94:995–1004. doi:10.1016/j.compstruct.2011.11.005.

[15] Thummalapalli VK, Donaldson SL. Biomimetic Composite Structural T-joints. J Bionic Eng 2012;9:377–84. doi:10.1016/S1672-6529(11)60130-3.

[16] Cartié DDR, Dell'Anno G, Poulin E, Partridge IK. 3D reinforcement of stiffener-to-skin T-joints by Z-pinning and tufting. Eng Fract Mech 2006;73:2532–40. doi:10.1016/j.engfracmech.2006.06.012.
[17] Koh TM, Feih S, Mouritz a. P. Experimental determination of the structural properties and strengthening mechanisms of z-pinned composite T-joints. Compos Struct 2011;93:2222–30. doi:10.1016/j.compstruct.2011.03.009.
[18] Przekop A. Design and Analysis of a Stiffened Composite Structure Repair Concept. 52nd AIAA/ASME/ASCE/AHS/ASC Struct. Struct. Dyn. Mater. Conf., Reston, Virigina: American Institute of Aeronautics and Astronautics; 2011, p. 1–22. doi:10.2514/6.2011-1912.
[19] White SR, Sottos NR, Geubelle PH, Moore JS, Kessler MR, Sriram SR, et al. Autonomic healing of polymer composites. Nature 2001;409:794–7. doi:10.1038/35057232.
[20] O'Brien T. Assesment of Composite Delamination Self-Healing Under Cyclic Loading. ICCM-17 17th Int Conf Compos Mater 2009.
[21] Bleay S., Loader C., Hawyes V., Humberstone L, Curtis P. A smart repair system for polymer matrix composites. Compos Part A Appl Sci Manuf 2001;32:1767–76. doi:10.1016/S1359-835X(01)00020-3.
[22] Trask RS, Bond IP. Biomimetic self-healing of advanced composite structures using hollow glass fibres. Smart Mater Struct 2006;15:704–10. doi:10.1088/0964-1726/15/3/005.
[23] Huang C-Y, Trask RS, Bond IP. Characterization and analysis of carbon fibre-reinforced polymer composite laminates with embedded circular vasculature. J R Soc Interface 2010;7:1229–41. doi:10.1098/rsif.2009.0534.
[24] Zako M, Takano N. Intelligent Material Systems Using Epoxy Particles to Repair Microcracks and Delamination Damage in GFRP. J Intell Mater Syst Struct 1999;10:836–41. doi:10.1106/YEIH-QUDH-FC7W-4QFM.
[25] Meure S, Furman S, Khor S. Poly[ethylene-co-(methacrylic acid)] Healing Agents for Mendable Carbon Fiber Laminates. Macromol Mater Eng 2010;295:420–4. doi:10.1002/mame.200900345.
[26] Norris CJ, Bond IP, Trask RS. The role of embedded bioinspired vasculature on damage formation in self-healing carbon fibre reinforced composites. Compos Part A Appl Sci Manuf 2011;42:639–48. doi:10.1016/j.compositesa.2011.02.003.
[27] Norris CJ, Meadway GJ, O'Sullivan MJ, Bond IP, Trask RS. Self-Healing Fibre Reinforced Composites via a Bioinspired Vasculature. Adv Funct Mater 2011;21:3624–33. doi:10.1002/adfm.201101100.
[28] Norris CJ, Bond IP, Trask RS. Interactions between propagating cracks and bioinspired self-healing vascules embedded in glass fibre reinforced composites. Compos Sci Technol 2011;71:847–53. doi:10.1016/j.compscitech.2011.01.027.
[29] ASTM. ASTM D6272-10, "Standard Test Method for Flexural Properties of Unreinforced and Reinforced Plastics and Electrical Insulating Materials by Four-Point Bending." Pennsylvania: ASTM International; 2010. doi:10.1520/D6272-10.
[30] ASTM. ASTM D5528-13, "Standard Test Method for Mode I Interlaminar Fracture Toughness of Unidirectional Fiber-Reinforced Polymer Matrix Composites," Pennsylvania: ASTM International; 2013. doi:10.1520/D5528-13.2.

Figures

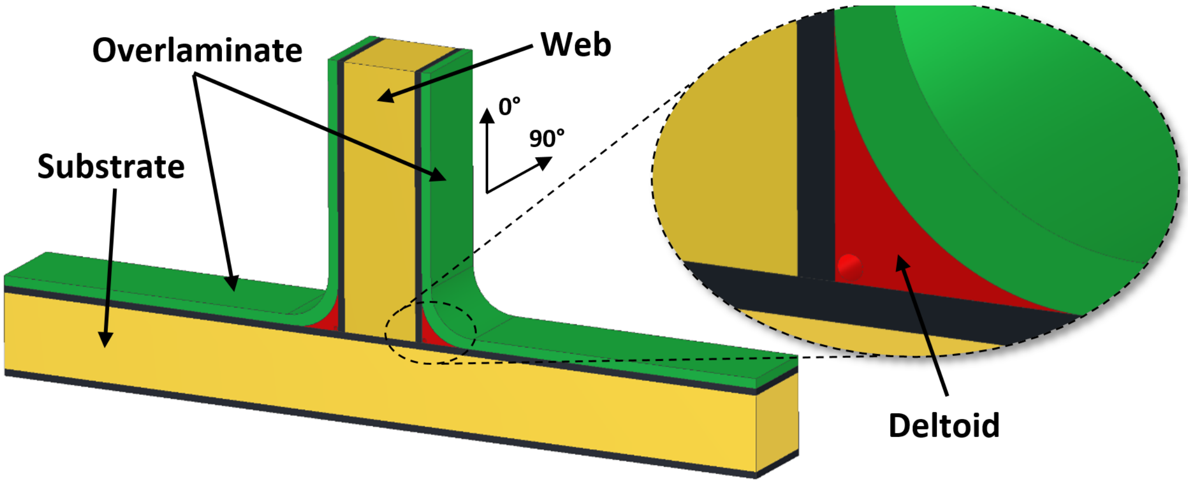

Fig. 1. Typical sandwich t-joint. The deltoid fillet (red) is an ideal candidate location for the deployment of a self-healing vascular network.

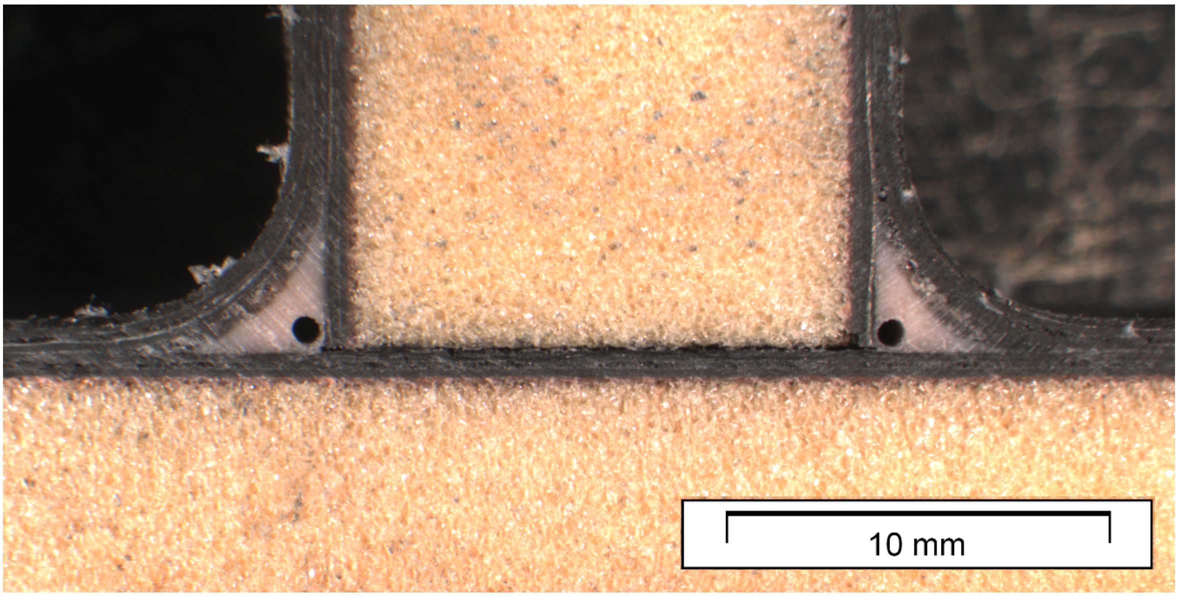

Fig. 2.

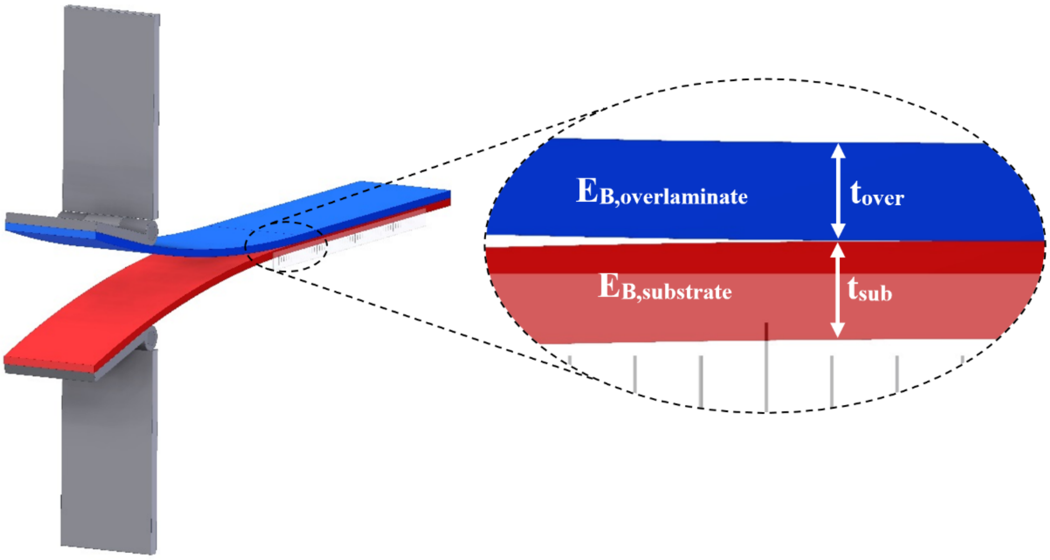

Fig. 3. Dissimilar DCB specimen. Overlaminate plies co-bonded to substrate using vacuum assisted wet layup.

Fig. 4. T-joint tensile test set up. Delamination along overlaminate/substrate interface of repaired vascularised T-joint sample (T2)

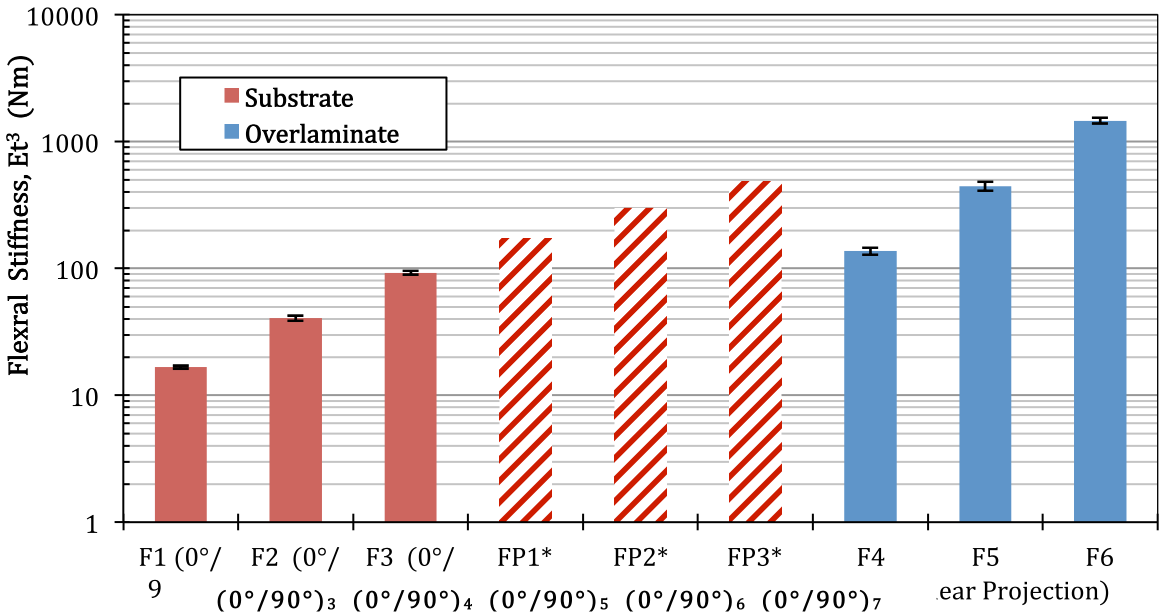

Fig. 5. Influence of thickness on apparent flexural stiffness of substrate (red) and overlaminate (blue) material. Stiffness of FP1-FP3 (red hatched) estimated by linear projection of F1-F3.

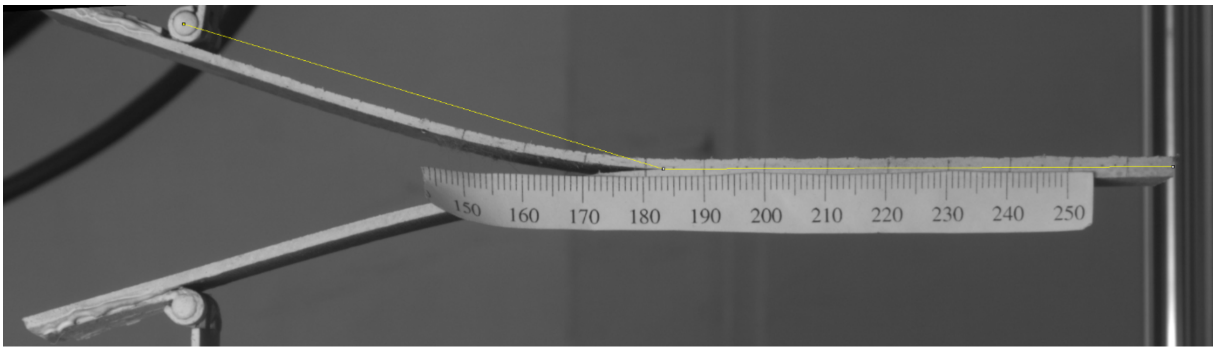

Fig. 6. Measurement of beam deflection using ImageJ analysis software

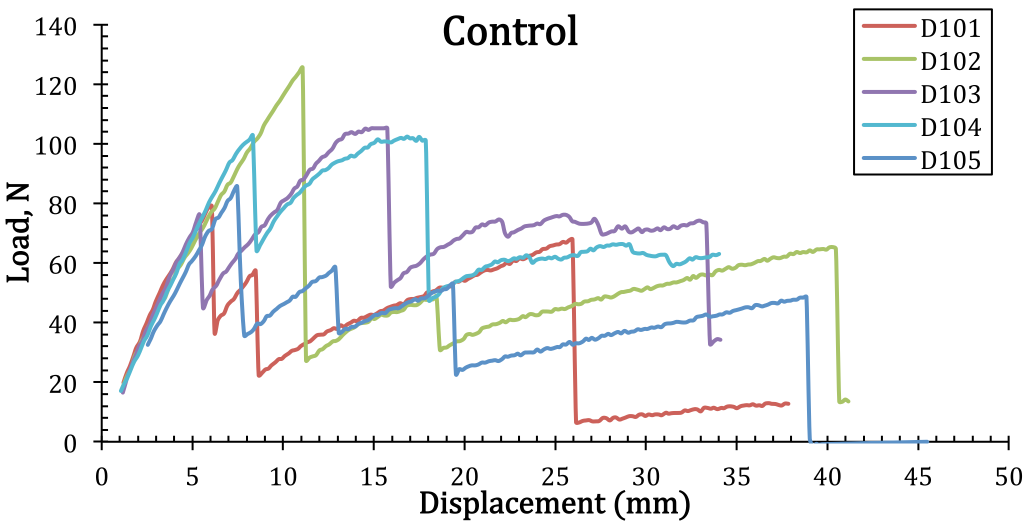

Fig. 7(a). Typical load-displacement trace for the unbalanced DCB specimen. Stick-slip crack propagation makes determination of fracture toughness difficult.

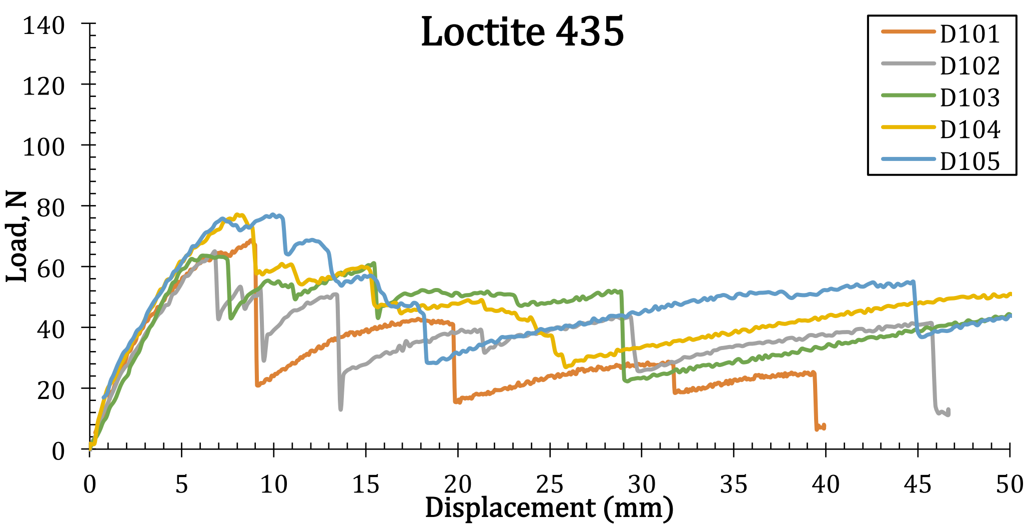

Fig. 7(b). Interfacial Mode I recovery from Loctite 435 cyanoacrylate

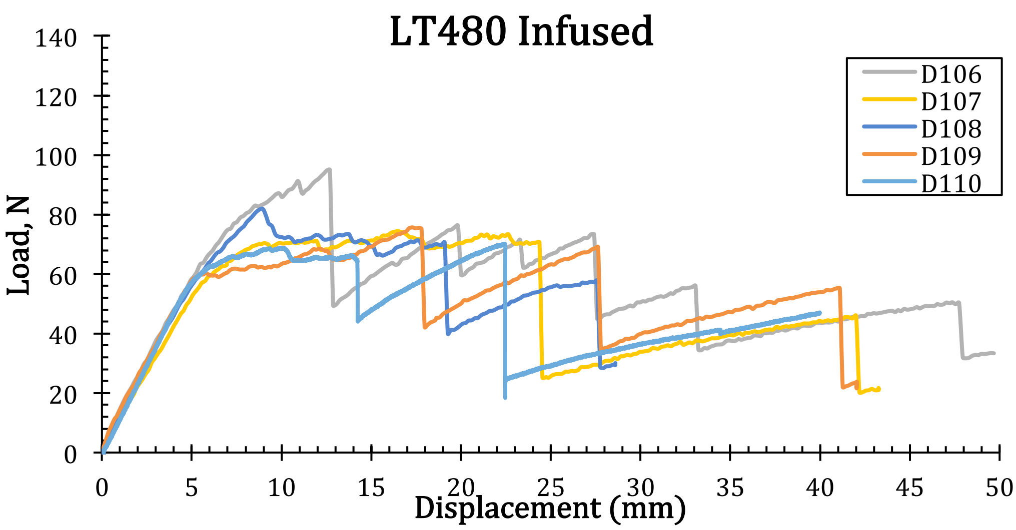

Fig. 7(c). Interfacial Mode I recovery from Loctite 480 cyanoacrylate

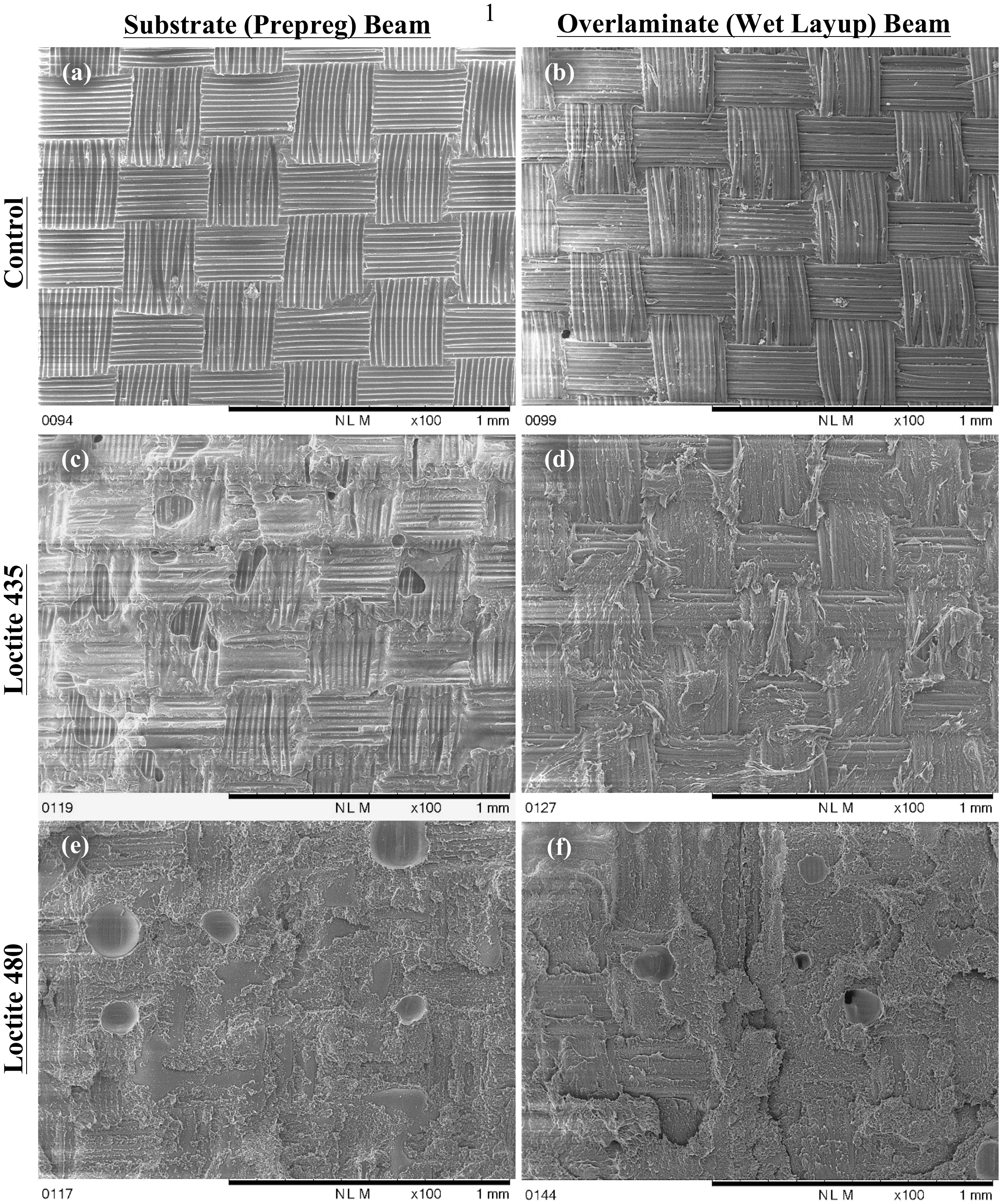

Fig. 8. Fracture morphology of dissimilar DCB specimens (a) resin rich surface showing imprint of fibres (b) exposed fibres showing delamination along fibre/matrix interface (c) voidage post repair (d) elongated material drawing consistent with ductile material response (e)&(f) textured morphology, uniform inclusions likely to be remnants from toughening phase.

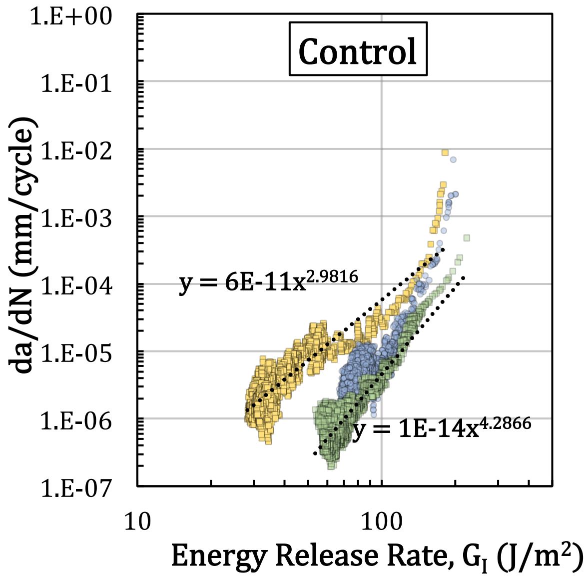

Fig. 9(a). Representative fatigue crack propagation showing variability within virgin (control) DCB dataset. Colours represent different samples within the same dataset.

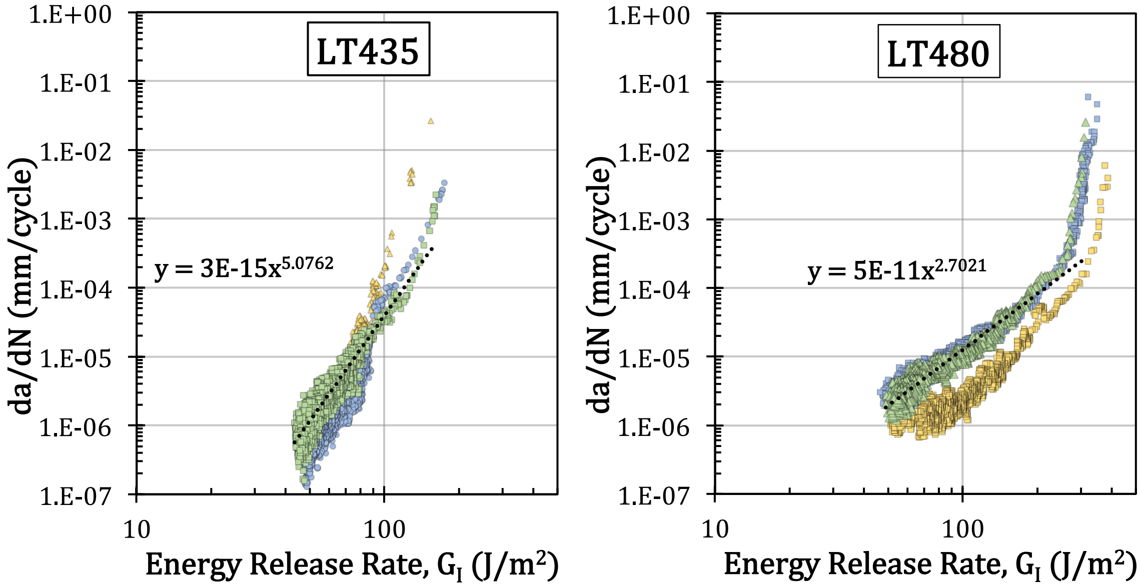

Fig. 9(b). Fatigue crack propagation of LT435 & LT480 CA infused DCB samples.

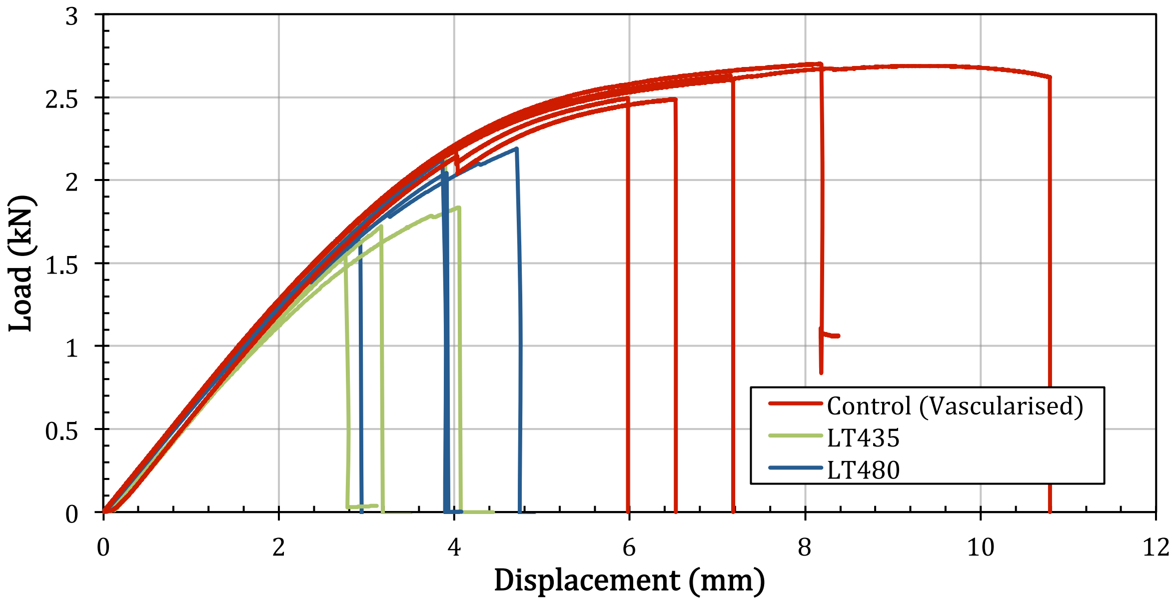

Fig. 10. Static strength of virgin and repaired T-joints.

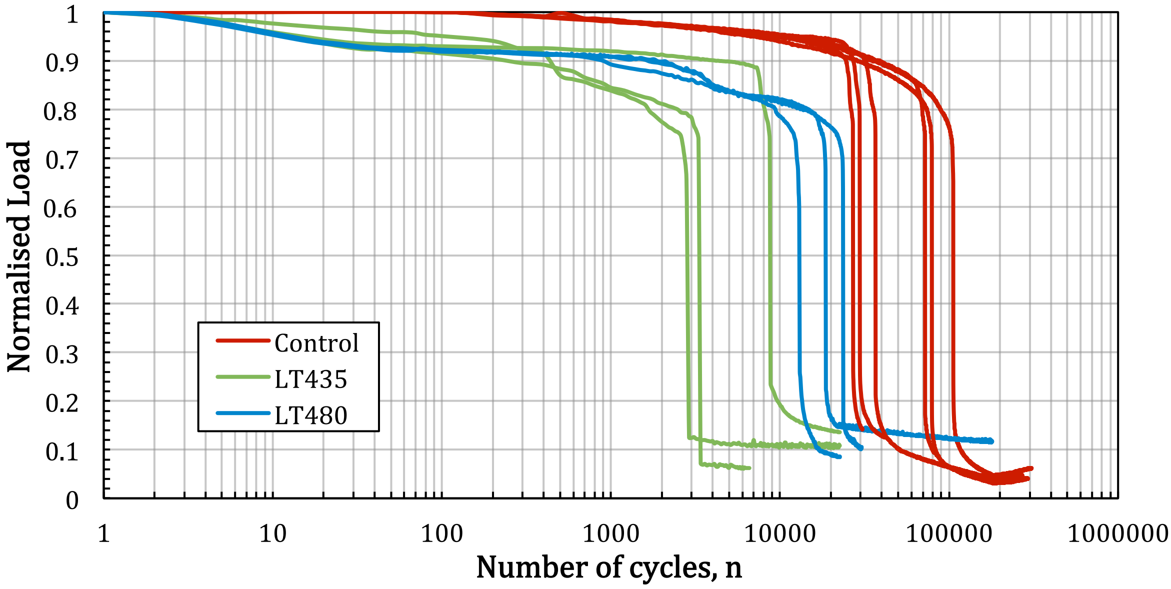

Fig. 11. Load bearing capacity under fatigue loading of control and repaired T-joints specimens. All results normalised to the peak load

Tables

Table 1. Fibre orientations and stacking sequences for T-joint (T) specimens (where 0° corresponds to the primary loading direction of the web or vertical overlaminate as shown in Fig. 1).

	Substrate / Web		Overlaminate		
ID	Stacking Sequence	Materials	Stacking Sequence	Materials	Vascules
T1	[(0°/90°)/+45°/-45°, HP200, -45°/°/+45°/(0°/90°)]$_T$	T700 VTM264	[(+45°/-45°)$_2$]$_T$	UT-C400 EC152/W2152	No
T2	“	“	“		1mm

Table 2. Layup and materials for DCB and Flexure specimens

ID	Fibre Orientation	Type	Fibre	Resin
D1	[(0°/90°)$_8$ / (0°/90°)/0°$_3$/(0°/90°)]$_T$	Prepreg / Wet Layup	-	-
F1	[(0°/90°)$_3$]$_T$	Prepreg	T700	VTM 264
F2	[(0°/90°)$_4$]$_T$	Prepreg	T700	VTM 264
F3	[(0°/90°)$_5$]$_T$	Prepreg	T700	VTM 264
F4	[(0°/90°)/0°$_2$*/(0°/90°)]$_T$	Wet Layup	UT-C300	EC152/W152
F5	[(0°/90°)/0°$_3$*/(0°/90°)]$_T$	Wet Layup	UT-C400 / UT-C300	EC152/W152
F6	[(0°/90°)/0°$_5$*/(0°/90°)]$_T$	Wet Layup	UT-C400 / UT-C300	EC152/W152

*Note 1 - Alternating ply weight. 0°$_2$ – 300/300, 0°$_3$ – 400/300/400gsm, 0°$_5$ – 400/300/400/300/400gsm

Table 3. Flexure specimen dimensions. All measurements in mm.

	Thickness	Support Length (L_s)		Specimen Length (L)		Width
ID	t (mm)	60:1	Nominal	60:1	Nominal	Nominal
F1	0.80	47.8	48	57.60	58	25
F2	1.01	60.5	60	72.00	72	25
F3	1.24	74.2	74	88.80	89	25
F4	1.42	84.9	85	101.9	102	25
F5	1.85	110.9	111	133.1	134	25
F6	2.52	151.2	151	181.5	182	25

Table 4. Strain energy release rate (G_{IC}) of control and infused DCB specimens

	Control		*Loctite 435*		*Loctite 480*	
	Initiation	*Propagation*	*Initiation*	*Propagation*	*Initiation*	*Propagation*
G_{IC} *(J/m^2)*	240-600	-	350 - 750	650 - 1100	650 - 1100	1250 - 1500

Table 5. Ultimate loads of virgin and repaired T-joints subject to 90° tensile pull-off.

Configuration	*Control*	*Vascularised*	*Loctite 435*	*Loctite 480*
Failure Load, kN	2.424	2.596	1.815	2.078
StdDev (CV,%)	0.121 (5.00)	0.092 (3.54)	0.207 (11.414)	0.276 (13.30)